Laboratory demonstration and characterization of phase-sorting interferometry

Gilles P.P.L. Otten[a], Matthew A. Kenworthy[a] and Johanan L. Codona[b]

[a]Leiden Observatory, P.O. Box 9513, 2300 RA Leiden, The Netherlands;
[b]Steward Observatory, University of Arizona, Tuscon, AZ 85721, USA

ABSTRACT

Non-common path (NCP) errors that lie downstream from the wavefront sensor (WFS) in an AO setup can't be directly corrected by the WFS and end up altering the science images by introducing quasi-static speckles. These speckles impose limits to the direct imaging of exoplanets, debris disks and other objects for which we require high contrast. Phase-sorting interferometry (PSI) uses WFS residuals as interferometric probes to the speckles. With the retrieved amplitude and phase the deformable mirror can be adjusted to remove the speckles. Previously PSI has been demonstrated to correct -to first order- the non-common path error on-sky at the MMTO in Arizona. We present an AO laboratory testbed and the techniques used to determine the properties of PSI; the influence of the time synchronisation between WFS and science camera, the achromacity of the atmosphere and other limiting factors. Furthermore we test the performance of the PSI method when coronagraphs such as apodizing phase plates, Lyot masks and 4QPMs are introduced to the setup. Lastly this setup enables us to rapidly prototype high-contrast imaging techniques.

Keywords: adaptive optics, high-contrast imaging, non-common path aberrations, focal-plane wavefront sensing

1. INTRODUCTION

Quasi-static speckles are an important limiting factor in reaching the contrast level required for the direct imaging of extrasolar planets.[1,2] Even if the wavefront sensor (WFS) could perfectly correct the wavefront, the science camera will see a slightly different optical path which will introduce a non-common path (NCP) aberration. Imperfections in the optics and telescope structure are therefore not corrected. A quasi-static background halo appears in the focal plane together with planet-like speckles. The timescale of the NCP aberration (on the order of seconds to minutes)[1] isn't fast enough to statistically average into a removable background nor is it static enough to remove using techniques like angular differential imaging (ADI)[3] and local optimization of combined images (LOCI).[4] One promising technique to characterise the non-common path aberrations is phase-sorting interferometry[5] (PSI). In this work we present the adaptive optics test bench at Leiden Observatory and the techniques that we will use to test the validity and limits of phase-sorting interferometry. The NCP aberration retrieval with PSI will be cross-checked against measurements taken with a modified Mach-Zehnder interometer and the differential optical transfer function technique (dOTF). The goal is to use a coronagraph and phase-sorting interferometry as a demonstrator for high contrast imaging with large telescopes LBT, VLT and E-ELT and reach a contrast in the lab of 10^{-5} at $2\lambda/D$ using only science images.

2. LABORATORY SETUP

An adaptive optics setup is used to characterize the non-common path aberrations (see Figure 1). Two different lasers are used in the setup; a 5 mW polarised red laser at 633 nm and a 0.5 mW polarised green laser at 543 nm. This reflects the current design of adaptive optic systems on telescopes where the wavefront sensor is fed by the visible part of the telescope beam while the instrument receives the longer (near-)infrared part. The two laser beams are combined with a beamsplitter and cleaned using a spatial filter consisting of a 20 mm microscope objective and 10 micron pinhole. This pinhole is reimaged onto a 20 mm pupil stop where the beam is distorted

otten@strw.leidenuniv.nl

Ground-based and Airborne Instrumentation for Astronomy IV, edited by Ian S. McLean, Suzanne K. Ramsay, Hideki Takami, Proc. of SPIE Vol. 8446, 84469F · © 2012 SPIE · CCC code: 0277-786X/12/$18 · doi: 10.1117/12.925839

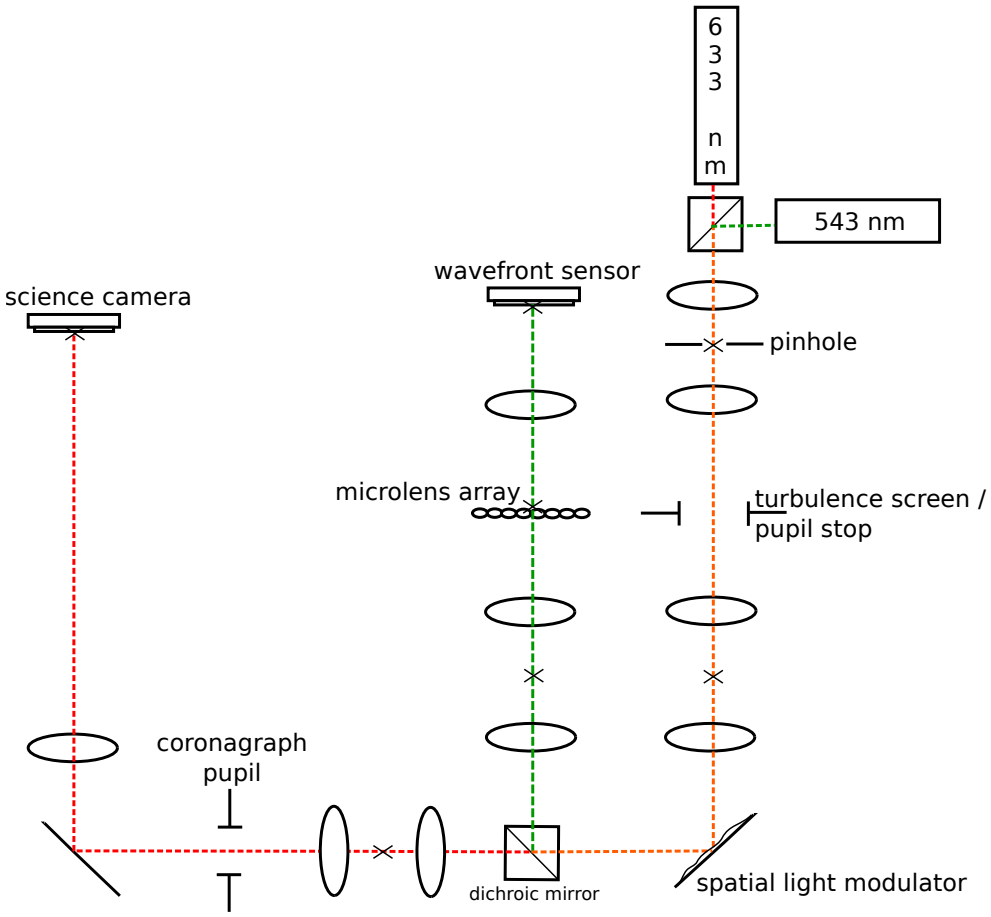

Figure 1. Schematic of the adaptive optics test bench. On the right, the 2 lasers, the spatial filter and turbulence screen. In the middle is the wavefront sensor branch and on the left is the science camera branch.

by a atmospheric turbulence plate. To correct the wavefront a liquid crystal spatial light modulator (SLM) is used. The SLM used was manufactured by Boulder Non-linear Systems and has a 512 by 512 pixel grid with 15 micron pitch. The previously mentioned pupil stop was reimaged as a 4 mm spot on the SLM. After the SLM the 2 different wavelengths were split using a dichroic into a wavefront sensor and a science camera branch.

2.1 Wavefront sensor branch

Within the wavefront sensor branch, the pupil is reimaged to 20 mm and passes through a 20 by 20 mm microlens array with a focal length of 40 mm and a pitch of 300 microns. The spots are then demagnified by a factor of 3 and imaged onto a Lumenera Lu125M 1280×1024 pixel CMOS camera with 6.7 micron sized pixels. The PSFs of the focal plane spots are therefore approximately 5 pixels across and 15 pixels apart.

2.2 Science camera branch

The reimaged pupil in the science camera branch has a diameter of 6 mm. The size of this pupil was chosen to match the size of the two coronagraphs that are available in our lab; The Apodizing Phase Plate[6,7] (APP) and the Vector-APP prototype.[8] With a 1000 mm lens the 6 mm pupil is focused onto a SBIG ST2000XM CCD camera. The chip has 1600×1200 pixels and 7.4 micron sized pixels. This converts into a full width half-maximum (FHWM) at 633 nm of 129 microns or approximately 17 pixels.

To convert the setup to an interferometer an extra path is added behind the coronagraph as can be seen in Figure 2. The interferometer gives an independent determination of the non-common path aberrations.

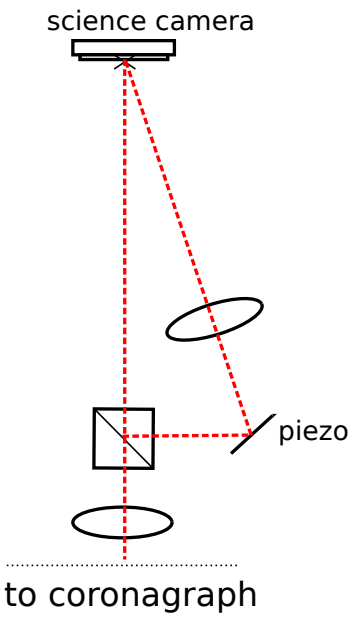

Figure 2. Modification of test bench that enables focal plane phase retrieval using the Modified Mach-Zehnder method described in Section 3.4. Part of the light is diverted using a beamsplitter and magnified. The magnification smooths the phase so it can be used as a flat phase reference to the PSF that contains NCP aberrations. The piezo element is used to step through a full wavelength of optical path difference in order to retrieve the phase and amplitude for each individual pixel in the focal plane.

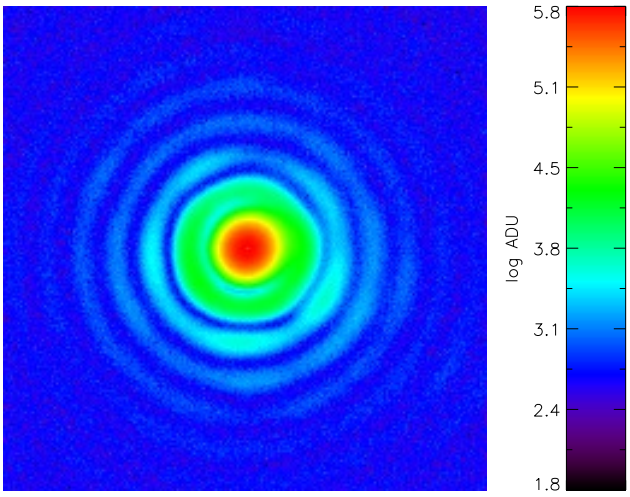

Figure 3. Stack of 20 exposures at the science camera of the point spread function with no turbulence plate and no coronagraph in the beam. Some astigmatism can be seen.

2.3 Data retrieval

Both cameras and the SLM can be controlled using modules in IDL. A stack of 20 images was obtained to test the performance of the setup without a turbulence plate and coronagraph and is seen in Figure 3.

3. REMOVING NON-COMMON PATH ABERRATIONS

The non-common path aberrations can be represented as a complex field in the pupil plane of the coronagraph. This field is added to the pupil field generated by the optics upstream of the dichroic splitter, and it includes the aberrations introduced by all the optics from the dichroic through to the science camera focal plane. This complex field can be decomposed as a series of sinusoidal ripples with a given amplitude, phase and orientation in the pupil plane. Each wave then transforms to a speckle in the science camera focal plane.

In order to confirm that the PSI method can correctly retrieve the NCP aberrations, the following four methods will be used to retrieve the NCP as a check of mutual consistency. The focus of these consistency tests will be the performance of the phase-sorting interferometry.

3.1 "Coffee rings method"

The key to PSI is the synchronization of the WFS telemetry and the science camera images. Short exposures typical of thermal infrared observations (100ms or less) show intensity variations along all the diffraction structures in the science images. If the WFS frames taken at the same time as the science camera frame are identified, a WFS wavefront can be reconstructed and Fourier transformed to produce a complex field at the science camera focal plane. The difference between this complex field and the intensity measurement at the focal plane is due to the NCP. These quantities can be respresented by vectors in the complex plane (see Figure 4) as the WFS vector (the green line) and the as yet unknown NCP vector (five possibilities represented by the blue lines). The science camera only gives the intensity, which is the amplitude squared of the electric field in the science camera focal plane. Because the amplitude is known but the phase is not, we can represent it in the complex plane with a circle with its radius equal to the amplitude (indicated in red). The WFS vectorially adds to the NCP to give a point on the red circle. Multiple exposures give new realizations for the science camera amplitude and the WFS vector, providing enough diversity to solve for the correct NCP for that pixel in the science camera focal plane (see Figure 5). This assumption is valid for small amplitude changes which are achieved when observing at Strehl ratios higher than 0.8.

To correct the difference in exposure times between science camera and WFS the complex image of the WFS is integrated to the same exposure time as the science camera. The quasi-static speckles vary on the order of seconds to minutes. Because the atmospheric speckles move in amplitude and phase on much shorter timescales, the time integrated vector arrow will move around the complex plane and gives multiple constraints on the non-common path aberrations. For a Shack-Hartmann WFS, there is an unknown scaling factor between the reconstructed phase screen and the true incident wavefront phase. To compensate for this difference a gain factor is introduced to the WFS vector that is assumed to be fixed for each pixel and only introduces one extra degree of freedom.

3.2 Phase-sorting interferometry

Similarly, when the residuals of the atmospheric speckles vary, they occasionally have the correct phase to null out a quasi-static speckle. Because we know the phase of the atmospheric speckles we can plot for a single pixel in multiple frames the intensity and the phase. If this is done on timescales shorter than the timescale of the quasi-static speckle an image will slowly build up where the intensity is lowest out of phase and highest in phase. In Figure 6 data can be seen from the CLIO imager at the 6.5 meter MMT which demonstrates this. The phase of the quasi-static speckle can easily be seen in Figure 6, the amplitude on the other hand is a combination of the amplitude of the quasi-static speckle and the amplitude of the static halo. Luckily the statistics of the science images can be used to quantify the contribution of the static halo.

Instead of building and fitting the image as seen in Figure 6 for each individual pixel it is also possible construct a software-based phase-stepping interferometer.[5] We construct four empty images as large as the science camera image. The intensities of each pixel taken at the science camera are added to one of these four images I_X according to the WFS phase that that pixel has. Each of the four images spans a phase range of $\pi/2$ centered around $\{0, \pi/2, \pi, 3 \cdot \pi/2\}$. We also have 4 images N_X that are incremented by one each time a pixel is added to one of the 4 phase maps. After gathering enough statistics we can construct a complex image ξ using Equation 1.

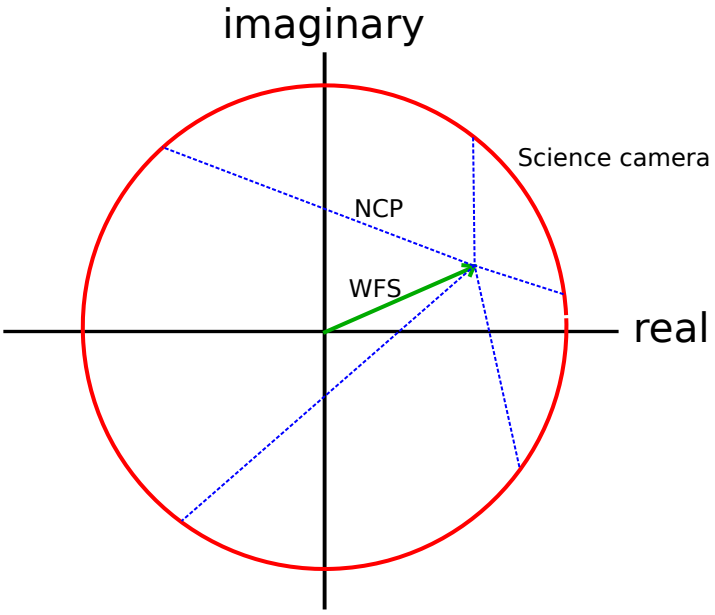

Figure 4. Determining NCP aberrations with the "coffee rings" method. In green is the wavefront sensor vector derived from the WFS telemetry. In red is the amplitude seen by the science camera. The difference between these two is the non-common path aberration (seen in blue as five potentially correct solutions). One image alone isn't enough to constrain the NCP.

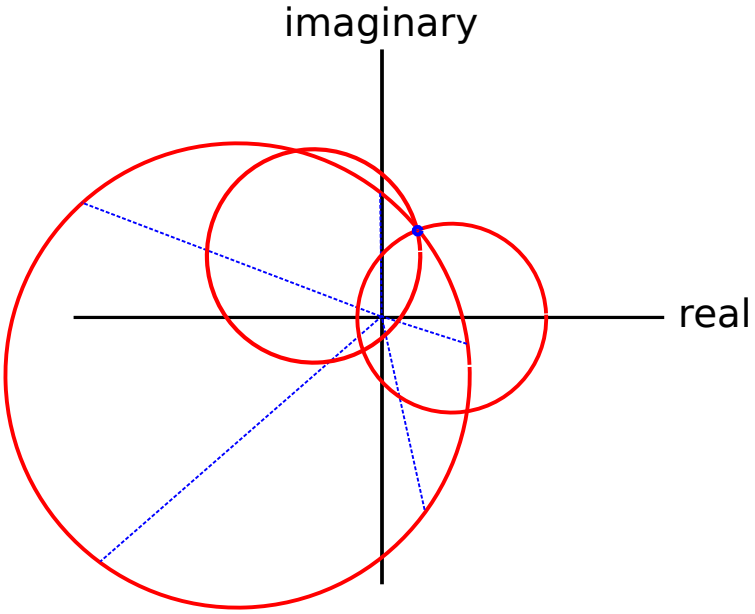

Figure 5. Taking the difference between the amplitude circle and the WFS vector is similar to translating the circle over the length of the WFS vector. When multiple measurements are taken in a short timespan, the NCP aberration doesn't change. The WFS vector and science camera intensity do change. Therefore although the circles will move around they will have a common point of intersection and this shows the true vector (complex number) of the NCP error.

$$\xi = \left(\frac{I_0}{N_0} - \frac{I_{180}}{N_{180}}\right) + i \cdot \left(\frac{I_{90}}{N_{90}} - \frac{I_{270}}{N_{270}}\right) \tag{1}$$

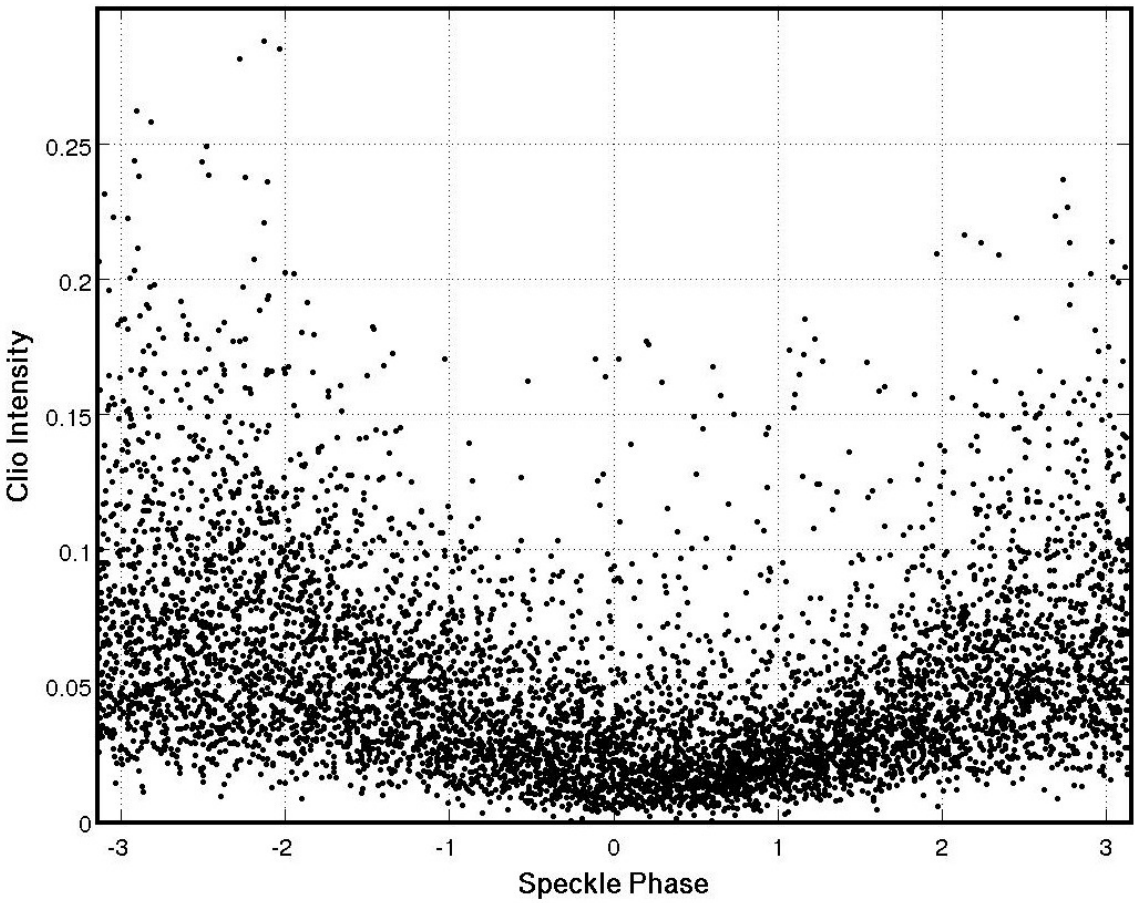

Figure 6. MMT data for a single pixel in the first Airy ring of a 7th magnitude star imaged with the infrared CLIO detector.[9] It can be seen that for this pixel the minimum of intensity is located at a WFS speckle phase of about 0.3 radians.[10]

The phase of this complex image ξ is equal to the phase of the NCP aberration. The amplitude is equal to the RMS of the WFS halo multiplied by the amplitude of the NCP aberrations.

3.3 Differential optical transfer function

A method developed by J.L Codona and presented[11] at this conference describes the full complex field retrieval through the use of optical transfer functions (OTF). Two images are taken in focus at the science camera, one image with a fully illuminated pupil and one where a small pointlike piece is blocked. The blocking can be done by inserting a sharp object at the edge of the pupil. The OTFs of both images are made by taking the fourier transform of their respective PSFs. The difference between the two OTFs is equal to the convolution of the difference between the two pupils ($\sim$delta peak) and the complex pupil field. The phase of this complex differential optical transfer function (dOTF) is equal to the phase of the pupil as seen from the science camera. To get a good signal-to-noise ratio on the dOTF and its phase a lot of light is needed which makes this method unpractical for most on-sky applications. However because this method only requires two images it is a quick method of determining aberrations in an optical setup. Especially because the supply of light can be easily tuned in a test bench.

The dOTF method was applied to the test bench at Leiden Observatory in order to retrieve the pupil phase map. In order to create a delta-like disturbance in the pupil the sharp tip of a metal file was inserted at the edge of it. The previously described method was used to calculate the dOTF which can be seen in Figure 7 and shows that our current system has a Strehl ratio of 83%.

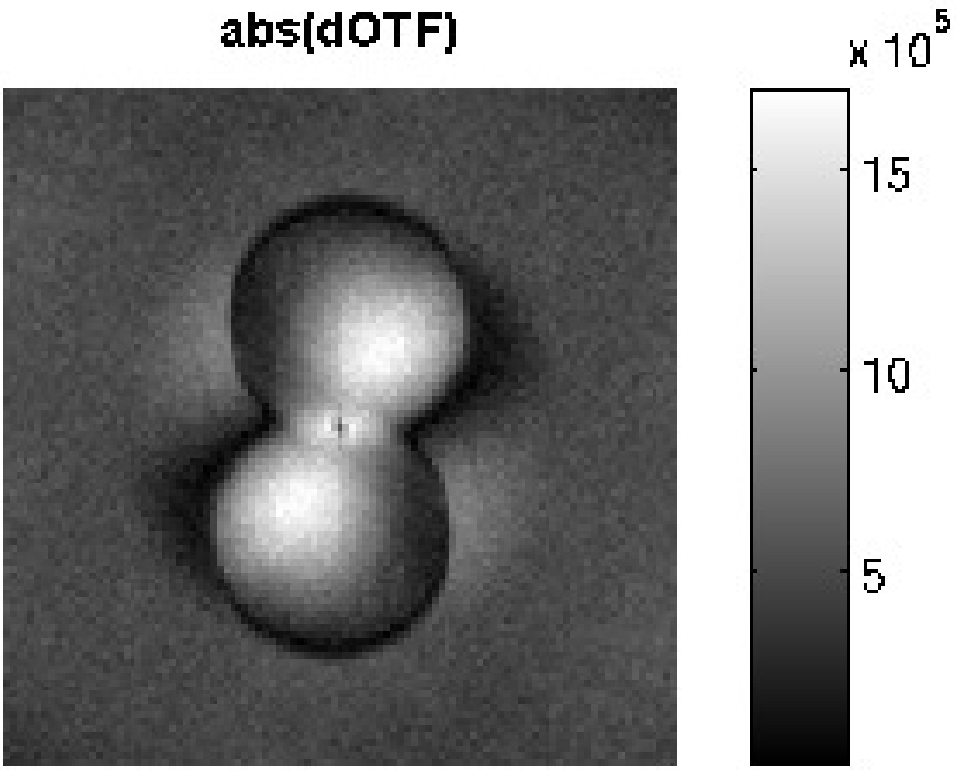

Figure 7. Top left shows the complex dOTF where brightness indicates amplitude and color indicates phase. In order to reduce the contrast the brightness in this frame has been scaled with a power law with $\gamma = 4$. Top right frame shows amplitude component of the dOTF. This amplitude is the amplitude map of the pupil. Lower right frame shows phase map in radians.

3.4 Angel-Mach-Zehnder interferometer

Another method to derive the non-common path aberration is to build an Angel-Mach-Zehnder interferometer[12] (see Figure 2). An image of the beam is taken away using a beamsplitter, magnified several times to smoothen and flatten the phase of the central portion of the beam and directly recombined with the rest of the light on the science camera. Due to the image magnification of the Airy core the phase of the reference beam will become uniform in phase, the eventual PSF on the science camera interferes with the magnified core and creates fringes. After stepping through a full wavelength of path length in the reference beam, the fringe pattern shifts after each step and can be converted back to the phase difference between the two paths.

3.5 Dialing out speckles

When we know the amplitude, phase and position of each of the quasi static speckles we can add sine waves with the deformable mirror (DM) that will destructively interfere with each speckle and perform speckle nulling, creating higher contrasts that will ultimately lead to 10^{-5} at separations of $1 - 2\lambda/D$.

4. CONCLUSIONS AND FUTURE WORK

We have described the layout of our optical testbed in Leiden Observatory, and have shown the first results of characterizing our optical performance with the application of dOTF in our system, which gives a Strehl of 83%.

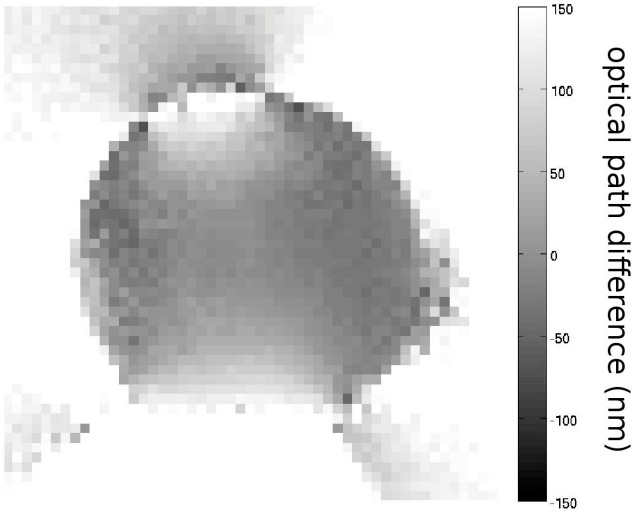

Figure 8. Optical path difference map in nanometers derived from the phase map shown in Figure 7 by dividing through 2π and multiplying by the wavelength $\lambda = 633$ nm, equivalent to a Strehl ratio of 83%. Some astigmatism can be seen in the retrieved phase map which is also seen in PSF image in Figure 3.

We are aiming for a Strehl of greater than 90%, representative of Strehls expected on the next generation of 35m class telescopes with instruments such as METIS, MICADO and EPICS.

Our close range goals include getting PSI working in the Leiden Optical Testbed, then introducing an APP coronagraph designed to work in the visible band at 820nm. The goal is to get 10^{-5} contrast at the smallest inner working angles, consistent with the expected performance of wavefront sensors on E-ELTs.[13] The additon of the Angel-Mach-Zehnder provides a consistency check between the PSI and the dOTF methods, where the PSI and AMZ provide a complete complex pupil field solution, and the dOTF can provide partial complex field solutions (limited by the overlap region introduced by the perturbation).

One of the long-term goals of the Leiden Optical Testbed is to demonstrate PSI with a coronagraph and to produce a set of software packages to implement PSI on current AO-enabled telescopes. The software library is expected to be coded in Python. PSI can provide reconstructed science PSFs for each science camera frame, but ultimately it can act as an additional anti-halo server to provide real time focal plane wavefront sensing at current telescopes with no additonal hardware cost.

ACKNOWLEDGMENTS

The authors would like to thank Remko Stuik for his help and support. This work is part of the research programme Instrumentation for the E-ELT, which is partly financed by the Netherlands Organisation for Scientific Research (NWO).

REFERENCES

[1] Hinkley, S., Oppenheimer, B. R., Soummer, R., Sivaramakrishnan, A., Lewis C. Roberts, J., Kuhn, J., Makidon, R. B., Perrin, M. D., Lloyd, J. P., Kratter, K., and Brenner, D., "Temporal evolution of coronagraphic dynamic range and constraints on companions to vega," *The Astrophysical Journal* **654**(1), 633 (2007).

[2] Martinez, P., Loose, C., Aller Carpentier, E., and Kasper, M., "Speckle temporal stability in xao coronagraphic images," *A&A* **541**, A136 (2012).

[3] Marois, C., Lafrenière, D., Doyon, R., Macintosh, B., and Nadeau, D., "Angular Differential Imaging: A Powerful High-Contrast Imaging Technique," *ApJ* **641**, 556–564 (Apr. 2006).

[4] Lafrenière, D., Marois, C., Doyon, R., Nadeau, D., and Artigau, É., "A New Algorithm for Point-Spread Function Subtraction in High-Contrast Imaging: A Demonstration with Angular Differential Imaging," *ApJ* **660**, 770–780 (May 2007).

[5] Codona, J. L., Kenworthy, M. A., and Lloyd-Hart, M., "A novel WFS technique for high-contrast imaging: Phase Sorting Interferometry (PSI)," in [*Society of Photo-Optical Instrumentation Engineers (SPIE) Conference Series*], *Society of Photo-Optical Instrumentation Engineers (SPIE) Conference Series* **7015** (July 2008).

[6] Codona, J. L., Kenworthy, M. A., Hinz, P. M., Angel, J. R. P., and Woolf, N. J., "A high-contrast coronagraph for the MMT using phase apodization: design and observations at 5 microns and 2 λ/D radius," in [*Society of Photo-Optical Instrumentation Engineers (SPIE) Conference Series*], *Society of Photo-Optical Instrumentation Engineers (SPIE) Conference Series* **6269** (July 2006).

[7] Kenworthy, M. A., Codona, J. L., Hinz, P. M., Angel, J. R. P., Heinze, A., and Sivanandam, S., "First On-Sky High-Contrast Imaging with an Apodizing Phase Plate," *ApJ* **660**, 762–769 (May 2007).

[8] Snik, F., Otten, G., Kenworthy, M., Miskiewicz, M., Escuti, M., Packham, C., and Codona, J., "The Vector-APP: a Broadband Apodizing Phase Plate that yields Complementary PSFs," *ArXiv e-prints* (July 2012).

[9] Sivanandam, S., Hinz, P. M., Heinze, A. N., Freed, M., and Breuninger, A. H., "Clio: a 3-5 micron AO planet-finding camera," in [*Society of Photo-Optical Instrumentation Engineers (SPIE) Conference Series*], *Society of Photo-Optical Instrumentation Engineers (SPIE) Conference Series* **6269** (July 2006).

[10] Codona, J. L., Kenworthy, M. A., and Hinz, P. M., "Focal plane wavefront sensing using AO speckles," (in preparation).

[11] Codona, J. L., "Theory and application of differential OTF (dOTF) wavefront sensing," in [*Society of Photo-Optical Instrumentation Engineers (SPIE) Conference Series*], *Society of Photo-Optical Instrumentation Engineers (SPIE) Conference Series* **8447** (July 2012).

[12] Codona, J. L. and Angel, R., "Imaging extrasolar planets by stellar halo suppression in separately corrected color bands," *The Astrophysical Journal Letters* **604**(2), L117 (2004).

[13] Guyon, O., Martinache, F., Cady, E. J., Balasubramanian, K., Belikov, R., Clergeon, C. S., and Mateen, M., "How ELTs will acquire the first spectra of rocky habitable planets," in [*Society of Photo-Optical Instrumentation Engineers (SPIE) Conference Series*], *Society of Photo-Optical Instrumentation Engineers (SPIE) Conference Series* **8447** (July 2012).